Journal of Alloys and Compounds 525 (2012) 184–190

Contents lists available at SciVerse ScienceDirect

Journal of Alloys and Compounds

journal homepage: www.elsevier.com/locate/jallcom

Effect of Ca^{2+} or Mg^{2+} additions on the electrical properties of yttria doped ceria electrolyte system

R.A. Montalvo-Lozano[a], S.M. Montemayor[a], K.P. Padmasree[b,*], A.F. Fuentes[b]

[a] Facultad de Ciencias Químicas, Universidad Autónoma de Coahuila, Bvd. Venustiano Carranza s/n, 25280 Saltillo, Coahuila, Mexico
[b] Cinvestav Unidad Saltillo, Apartado Postal 663, 25000 Saltillo, Coahuila, Mexico

ARTICLE INFO

Article history:
Received 3 October 2011
Received in revised form 31 January 2012
Accepted 5 February 2012
Available online xxx

Keywords:
Conductivity
Ceramic
Oxides
Electrolytes

ABSTRACT

The effect of Ca^{2+} or Mg^{2+} co-doping on the electrical conductivity of ceria–yttria electrolytes of general formulae $Ce_{0.9}Y_{0.1-x}M_xO_{2-\delta}$ ($x = 0$, 0.05) and $Ce_{0.85}Y_{0.15-x}M_xO_{2-\delta}$ ($x = 0$, 0.05, 0.1) (M = Ca or Mg) were investigated. Powder samples were synthesized by mechanical milling. The phase identification, microstructures, and ionic conductivities of the samples were studied by X-ray diffraction, scanning electron microscopy and AC impedance spectroscopy. The results showed that in comparison to singly doped ceria, co-doping with appropriate ratio of Y^{3+} and Ca^{2+} or Mg^{2+} showed higher conductivities and lower activation energies. For CaO co-doped system, conductivity of the samples improves as the concentration of the dopant increases and maximum conductivity is obtained for the composition $Ce_{0.85}Y_{0.05}Ca_{0.1}O_{1.875}$. But for MgO co-doped system, Mg = 5 mole% show better electrical properties further addition leads to a decreases in the conductivity. The electrical properties of grain boundary have a large influence due to co-doping than that of the bulk.

1. Introduction

Solid oxide fuel cells (SOFCs) have attracted considerable attention for distributed power sources due to its high efficiency and low emission of pollutions to the environment [1,2]. They are energy conversion devices which produce electricity directly from the chemical conversion of a fuel gas and an oxidant through an electrochemical reaction. Currently yttria stabilized zirconia (YSZ) is widely used as an electrolyte due to its outstanding chemical and mechanical stabilities, but it requires high operating temperature (1000 °C) for the cell operation. High operating temperature of YSZ electrolyte can lead to complex material problems like the need of high cost interconnector and other construction materials, interfacial diffusion between electrolyte and electrodes, long term stability, etc. Therefore the development of solid electrolytes that can be used in the intermediate temperature range (e.g., 600–800 °C) is important for the potential development of solid oxide fuel cell technology. Many studies have been conducted on other materials with high oxide ion conductivity such as lanthanum gallate and ceria based electrolytes [3,4]. These materials have higher ionic conductivity in the intermediate temperature range compared to the conventional YSZ. Among these new materials, rare earth and alkaline earth materials doped ceria have been widely considered as the most promising electrolytes for intermediate temperature solid oxide fuel cells (IT-SOFC) [5]. Doping cerium with elements of valence different from that of Ce^{4+} leads to the incorporation of oxygen vacancies for charge compensation in the lattice structure. Ceria doped with Gd^{3+} or Sm^{3+} shows the highest ionic conductivity but yttria doped ceria is of particular interest due to its comparatively high value of ionic conductivity, relative abundance and low cost of yttrium oxide against samarium and gadolinium [6]. The structural modification of ceria based systems by co-doping is one possible way to improve the oxide ion conductivity depending on the chemical composition, although in some cases deterioration of the ionic conductivity or increased electronic conductivity was observed [7–9].

The total conductivity of a polycrystalline material consists of both bulk and grain boundary parts and the effect of grain boundary conduction on the performance of an electrolyte are very significant for intermediate and lower temperature applications. The bulk and grain boundary conductivity of the co-doped system varies considerably depending on the chemical nature of the dopants, their concentration and the oxidation state. The grain boundary effect in these polycrystalline samples has been mainly attributed to the presence of highly siliceous amorphous phases, but recent studies have demonstrated that high purity materials also show this effect and therefore cannot attributed only due to silica contamination [10]. Another possibility is the formation of space charge layer adjacent to the grain boundary is responsible for the low conductivity [11]. It is reported that the addition of alkaline earth oxides increases the grain boundary conductivity of doped ceria to a large extent [12]. The aim of this work is to study the co-doping

* Corresponding author. Tel.: +52 8444389612; fax: +52 8444389610.
E-mail address: padma512@yahoo.com (K.P. Padmasree).

0925-8388/$ – see front matter © 2012 Elsevier B.V. All rights reserved.
doi:10.1016/j.jallcom.2012.02.045

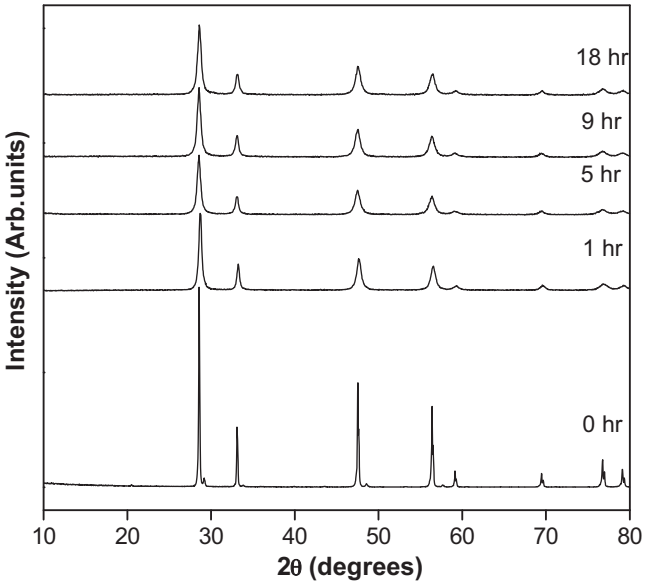

Fig. 1. X-ray powder diffraction patterns obtained at room temperature for $Ce_{0.9}Y_{0.1}O_{1.95}$ sample at different milling times.

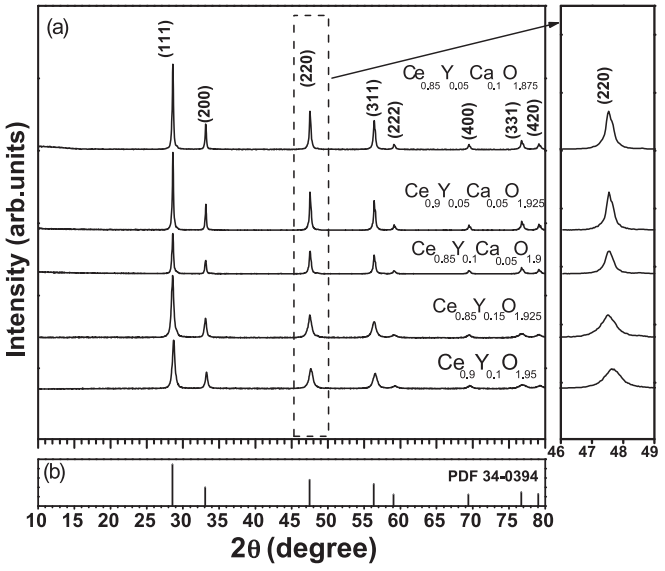

Fig. 2. X-ray powder diffraction patterns obtained after 1 h milling for the single and CaO co-doped samples (a), numbers in parenthesis are the Miller indexes of the main reflections of the fluorite crystal structure. The reported XRD pattern of cubic fluorite CeO_2 (PDF-ICDD 34-0394) is shown at the bottom (b). Right insert shows some part of the XRD patterns.

effect of alkaline earth elements like Ca^{2+} or Mg^{2+} to yttria doped ceria system on the ionic conductivity and sintering characteristics. To investigate the co-doping effect of calcium or magnesium on yttria doped ceria electrolyte, two groups of samples with general formulae $Ce_{0.9}Y_{0.1-x}M_xO_{2-\delta}$ ($x = 0$, 0.05) and $Ce_{0.85}Y_{0.15-x}M_xO_{2-\delta}$ ($x = 0, 0.05, 0.1$) (M = Ca or Mg) were prepared by mechanical milling process.

2. Experimental techniques

The solid solution with the formulae $Ce_{0.9}Y_{0.1-x}M_xO_{2-\delta}$ ($x = 0$, 0.05) and $Ce_{0.85}Y_{0.15-x}M_xO_{2-\delta}$ ($x = 0$, 0.05, 0.1) (M = Ca or Mg) was synthesized by mechanical milling, using high purity (Aldrich, >99+%) CeO_2, Y_2O_3, CaO and MgO as the starting materials. Stoichiometric mixtures of the above chemicals were placed in zirconia containers together with 20 mm diameter zirconia balls as grinding media (balls to powder mass ratio = 10:1). Dry mechanical milling was carried out in air in a planetary ball mill by using a rotating disc speed of 350 rpm. The relative density of the sintered samples was calculated from the ratio of the measured density by the Archimedes method and that of the theoretical density. The phase evolution on milling and the sintered sample was analyzed by using X-ray powder diffraction in Philips X'pert Diffractometer using Ni-filtered CuK_α radiation ($\lambda = 1.5418$ Å). The microstructure of the milled and sintered pellets was observed by scanning electron microscopy (SEM) in Philips XL30 ESEM microscope equipped with an EDAX Inc. energy dispersive X-ray detector for microanalysis. Specimens for electrical property measurements were pellets obtained by pressing the sample powder in a hydraulic press at a pressure of 5 MPa of 10 mm diameter and ~1 mm thickness. The resulting green pellets were placed in a platinum crucible and sintered at 1200 °C and 1500 °C for 5 h in air with a slow heating rate of 2 °C/min in all cases. The two electrodes were formed by applying platinum paste (SPI-Chem conductive platinum paint) to either surface of the pellets and then heat treated at 600 °C for two hours before the measurement to burn out the binder of the platinum paste and to ensure good contact of the electrodes with the pellet. The transport properties of the sintered pellets were examined by ac impedance spectroscopy over a frequency range 100 Hz to 1 MHz using an impedance analyzer of Solartron 1260 Frequency Response Analyzer in the temperature range 200–800 °C. The impedance data were analyzed by using the equivalent circuit of the Z-view software.

3. Result and discussions

Fig. 1 shows the XRD patterns of $Ce_{0.9}Y_{0.1}O_{1.95}$ sample selected as representative of the series, at different milling times. After 1 h milling there is a considerable decrease in intensity and broadening of the characteristic diffraction peaks as a result of the decrease in crystallite size and an increase in lattice strain taking place during milling. A single phase fluorite type material is obtained after milling for a time period of 1 h. With extended milling up to 18 h, the number and intensity of the characteristic reflections of fluorite phase remains the same with no additional peaks present. The XRD analysis of all the samples was done after 1 h of dry milling at room temperature to ensure the complete dissolution of dopants into CeO_2 lattice. Fig. 2 shows the XRD patterns obtained after 1 h of milling for the single and Ca^{2+} co-doped samples. The position of XRD peaks moved slightly towards lower angles with increasing Calcium. This is because the ionic radius decreases in the order Ca^{2+} (0.112 nm) > Y^{3+} (0.1019 nm) > Ce^{4+} (0.097 nm), so the substitution of Ce^{4+} with Y^{3+} and Ca^{2+} in the lattice of CeO_2 would enlarge the crystal lattice. Fig. 3 shows the XRD pattern of the sample $Ce_{0.85}Y_{0.05}Ca_{0.1}O_{1.875}$ after 1 h milling (a) and sintered at 1500 °C for 5 h (b). The XRD peaks of all the samples exhibited all major peaks

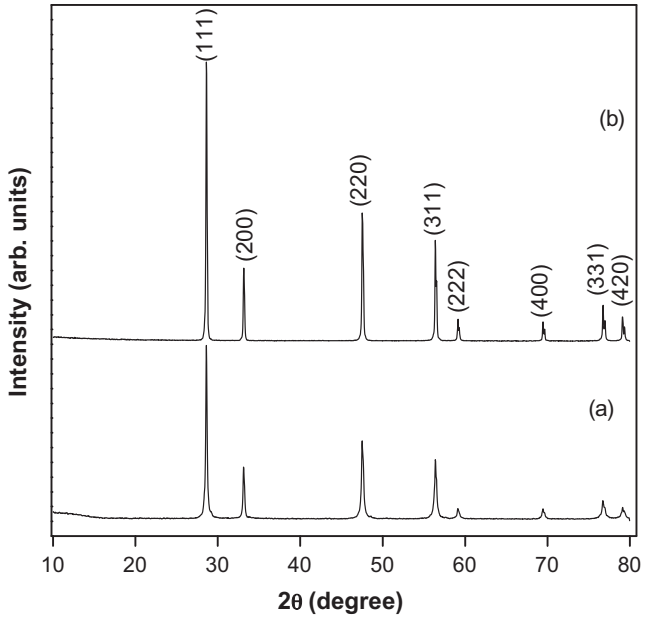

Fig. 3. XRD patterns obtained for the sample $Ce_{0.85}Y_{0.05}Ca_{0.1}O_{1.875}$ after (a) 1 h milling, (b) sintered at 1500 °C.

of a fluorite structure in ceria after 1 h of milling and sinterization. This may suggest that rare earth and alkaline earth oxides dissolved into ceria. Any additional phase corresponding to the dopants is not observed. XRD patterns of the sintered sample are same as that of the green sample except that the XRD peaks are more intense in the case of sintered sample. This implies that the sintering process helps to increase the crystal size and the increase of pellet compaction. The relative density of pellets measured by Archimedes method increases from 89% to 97% with the increase of sintering temperature from 1200 °C to 1500 °C, and it indicate that highly sinterable samples were synthesized by mechanical milling. The SEM micrographs of $Ce_{0.85}Y_{0.05}Ca_{0.1}O_{1.875}$ milled sample, and after sintered at 1200 °C and 1500 °C, are shown in Fig. 4. The just milled samples (Fig. 4(a)) have a uniform particle size distribution and well crystalline shape. Sintering at 1200 °C (Fig. 4(b)) yields grains of uniform size and shape with no evidence of exaggerated grain growth. It showed porous microstructures with grains smaller than 1 μm. Sample sintered at 1500 °C (Fig. 4(c)) shows a dense structure and well defined grains separated by grain boundaries. The grains of all the samples sintered at 1500 °C exhibit non uniform size and shapes. The scanning electron micrograph of $Ce_{0.85}Y_{0.05}Mg_{0.1}O_{1.875}$ sample sintered at 1500 °C is shown in Fig. 5, and inset of the figure shows the MgO phases (dark color) present at the grain boundary by EDAX analysis.

The ac impedance spectroscopy was applied to determine the electrical properties of singly and co-doped ceria based electrolyte samples. The real (Z') and imaginary (Z'') parts of the impedance can be determined by applying a small sinusoidal voltage across the sample and measuring the amplitude and phase angle of the current in a steady state condition. In an impedance plot, the frequency increases from right to the left across the plot. In an ideal case, ac impedance of an ionic conductor contains contributions from the bulk, grain boundaries and electrode–electrolyte interfaces, which can be reflected in a complex plane by three successive semi-circles. The intercept of the high frequency semicircle at the real axis represents the bulk resistance (R_b), low frequency intercept point of the intermediate frequency semicircle represents the grain boundary resistance (R_{gb}), and the intercept of low frequency semicircle is the electrode polarization resistance. The resistance value at different temperatures can be obtained from the impedance plot and it is then converted to bulk conductivity (σ_b), grain boundary conductivity (σ_{gb}) and total conductivity (σ_t) using the relation $\sigma = l/AR$, where l and A represent the sample thickness and electrode area of the sample surface, $R = R_b + R_{gb}$ is the total resistance obtained from the impedance plot respectively.

Fig. 6 shows the impedance spectra of (a) CaO and (b) MgO, co-doped ceria yttria system of the series $Ce_{0.9}Y_{0.1-x}M_xO_{2-\delta}$ ($x = 0$, 0.05) and $Ce_{0.85}Y_{0.15-x}M_xO_{2-\delta}$ ($x = 0$, 0.05, 0.1) sintered at 1500 °C in air. In the figure, two features can be observed, an incomplete depressed arc at high frequency and a part of the second arc at low frequency. The high frequency arc is due to resistive and capacitive effects of the bulk whereas the low frequency arc is related to the blocking of the charge carriers at grain to grain interfaces. From Fig. 6(a) we can see the bulk resistance associated with $Ce_{0.9}Y_{0.5}Ca_{0.5}O_{1.925}$ sample is less compared to other single and co-doped ceria systems at 250 °C. It also shows that grain boundary resistance decreases with the increase of Ca^{2+} addition to ceria yttria system. Fig. 6(b) shows the bulk resistance associated with MgO co-doped samples is less compared to the yttria doped ceria samples at 200 °C. It also shows for the series $Ce_{0.85}Y_{0.15-x}Mg_xO_{2-\delta}$, as the amount of Mg increases from 5 to 10 mole%, bulk resistance has a small effect compared to the grain boundary part. This may be attributed to the very low solubility of Mg^{2+} in the ceria yttria lattice and it can be seen from Fig. 5, that a good amount of Mg^{2+} segregate at the grain boundary and it effect the grain boundary properties. In an ideal case, frequency response of the

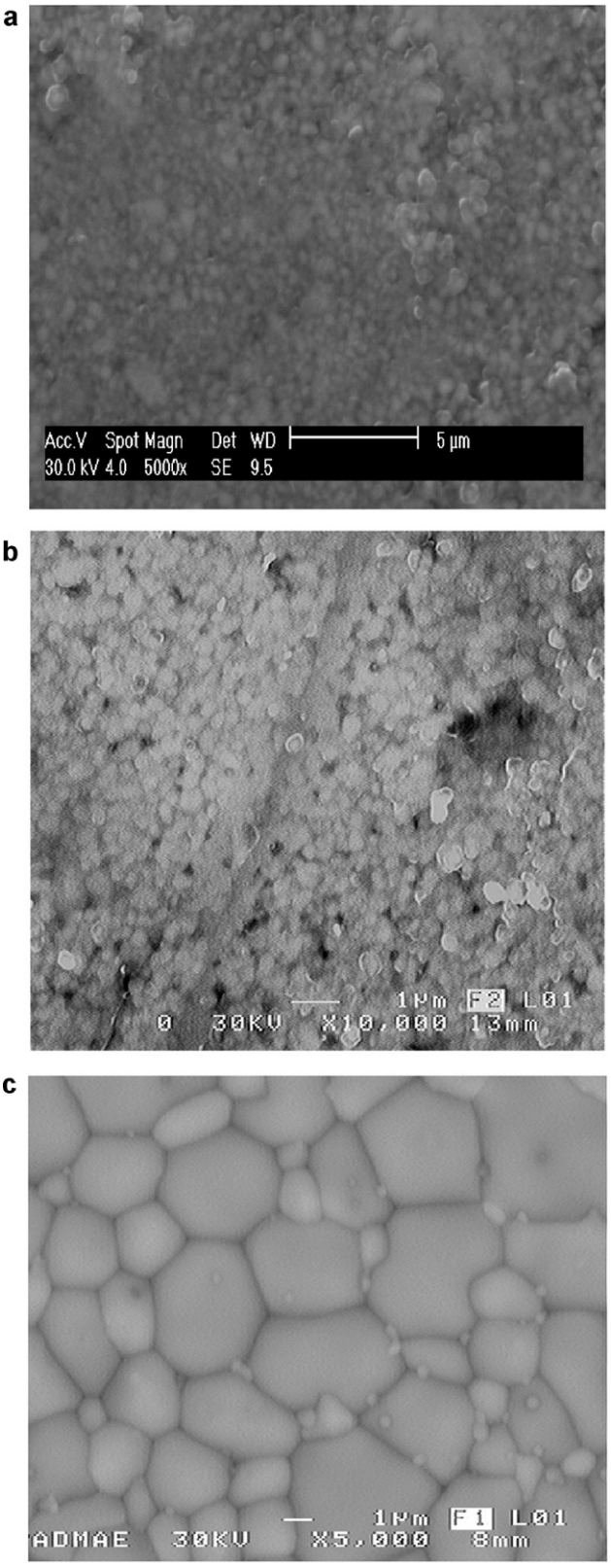

Fig. 4. Scanning electron micrograph of $Ce_{0.85}Y_{0.05}Ca_{0.1}O_{1.875}$ (a) just milled sample, and sample sintered at 1200 °C (b) and 1500 °C (c) for 5 h.

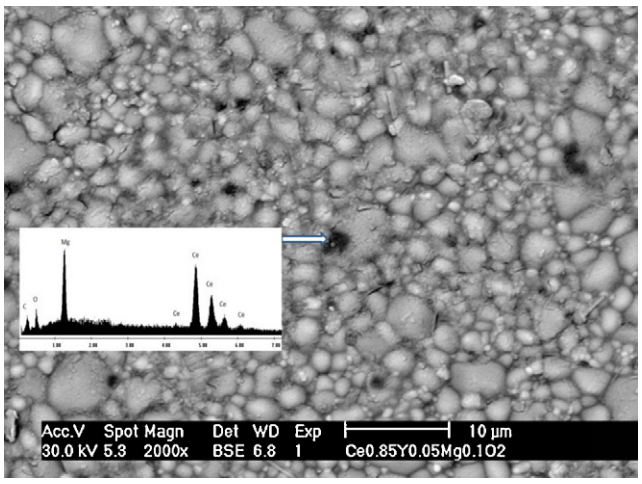

Fig. 5. Scanning electron micrograph of the composition $Ce_{0.85}Y_{0.05}Mg_{0.1}O_{1.875}$ sintered at 1500 °C for 5 h. The inset of Fig. 5 shows the EDAX analysis of the dark phase.

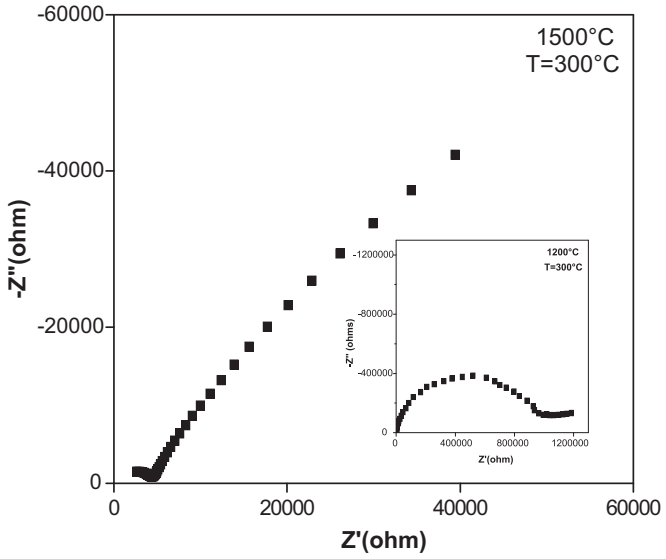

Fig. 7. Impedance diagrams of $Ce_{0.85}Y_{0.05}Mg_{0.1}O_{1.875}$ sample taken at 300 °C after sintering the green pellet at 1200 °C and 1500 °C.

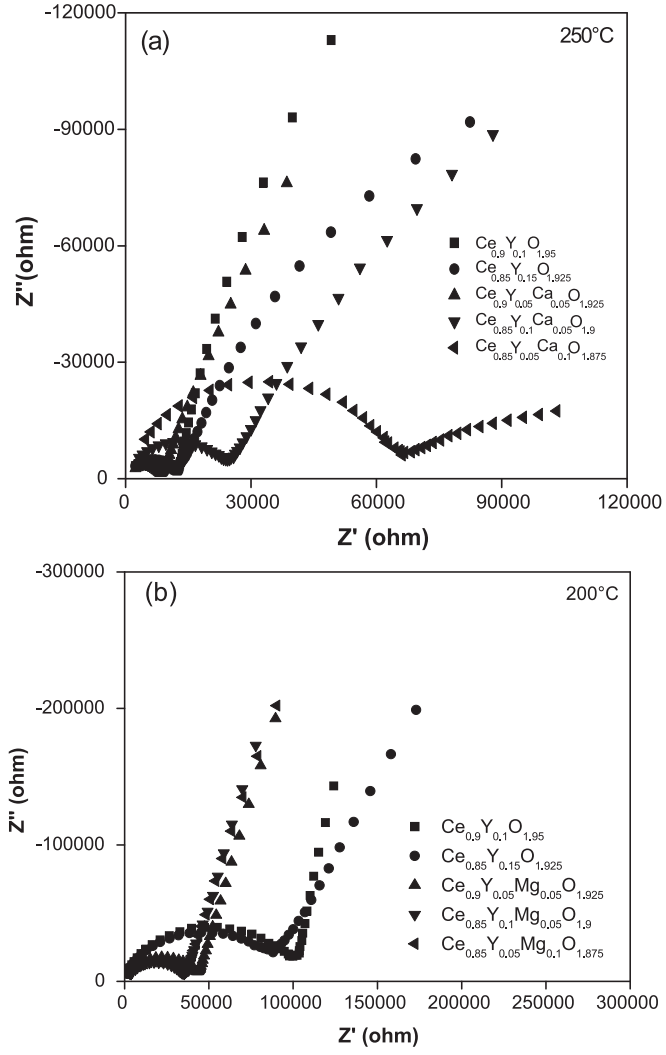

Fig. 6. Impedance spectra of (a) CaO co-doped and (b) MgO co-doped ceria–yttria system of the series $Ce_{0.9}Y_{0.1-x}M_xO_{2-\delta}$ ($x = 0$, 0.05) and $Ce_{0.85}Y_{0.15-x}M_xO_{2-\delta}$ ($x = 0$, 0.05, 0.1) sintered at 1500 °C in air.

bulk polarization of a polycrystalline electrolyte can be modeled as a resistor (R) and capacitance (C) pair in parallel. A parallel RC element represents a lossy capacitor with a typical relaxation time which corresponds to the process. However to model the experimental data in the present case, a constant phase element (CPE) is required in place of the capacitor. Constant phase element is equivalent to a distribution of capacitors in parallel and it accounts for the inhomogeneties of the sample and electrode microstructures. A series of resistances and constant phase elements (CPEs) were used to model the impedance spectra of the samples. As the measurement temperature is increased, bulk and grain boundary resistance cannot be separated because with the increase of temperature, the arcs are shifted into high frequencies, which lead to successive disappearance of bulk and grain boundary arc. It is reported that in most cases, the impedance spectra do not exhibit well resolved arcs for bulk and grain boundary contributions due to the limitations of the equipment and the strong influence of temperature on the bulk and grain boundary resistances. Therefore, it is possible to extrapolate the grain boundary resistance data and then subtract these values from the total resistance to estimate the bulk resistance [13–15].

Fig. 7 shows the complex impedance plot of $Ce_{0.85}Y_{0.05}Mg_{0.1}O_{1.875}$ sample sintered at 1200 °C and 1500 °C for 5 h. At low sintering temperature ($T = 1200$ °C), only one semicircle is observed, and with increasing the sintering temperature to 1500 °C, the contributions due to bulk, grain boundary and electrode–electrolyte interface is observed at 300 °C. Fig. 7 shows that sintering at 1500 °C results in rapid decrease of electrical resistance and the difference in bulk resistivity is higher than two orders of magnitude between the two specimens. The comparison of the co-doped samples with the same composition sintered at different temperatures clearly shows the samples sintered at 1500 °C shows higher values of electrical conductivity compared to the samples sintered at 1200 °C. The temperature dependence of electrical conductivity between the samples sintered at 1200 and 1500 °C is shown in Fig. 8, with the conductivity of the latter being higher than that of the former. The main reason for this difference could be related to a better solubilization and homogenization of the doped elements into the ceria matrix, grain growth and the removal of interconnected porosity with increase in sintering temperature.

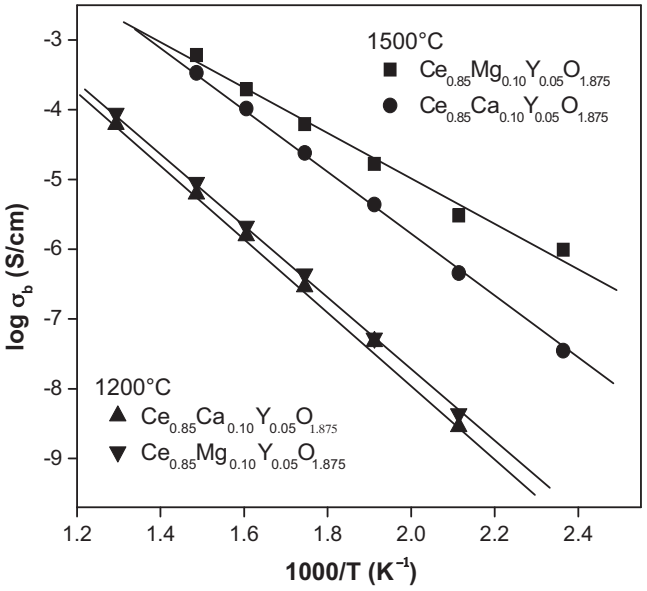

Fig. 8. Temperature dependence of electrical conductivity between the samples sintered at 1200 and 1500 °C.

The bulk, grain boundary and total conductivity of $Ce_{0.9}Y_{0.1-x}M_xO_{2-\delta}$ ($x = 0$, 0.05) and $Ce_{0.85}Y_{0.15-x}M_xO_{2-\delta}$ ($x = 0$, 0.05, 0.1) (M = Ca or Mg) samples sintered at 1500 °C are shown in Fig. 9(a)–(c). Since the electrical conduction in these materials is thermally activated, this type of process is appropriate to be analyzed by the Arrhenius equation:

$$\sigma = \frac{\sigma_0}{T} \exp\left(-\frac{E_a}{kT}\right) \quad (1)$$

where σ_0 is the pre-exponential factor being a constant in certain temperature range, k is the Boltzmann constant, T is the absolute temperature and E_a is the activation energy for ion migration, which is the sum of migration enthalpy (ΔH_m) and association enthalpy (ΔH_a). The activation energy for bulk, grain boundary and total conduction is calculated from the slope of the corresponding Arrhenius plot. The ionic conductivity increases as the temperature increases, whereas the difference in bulk ionic conductivity decreases with the increase of temperature. The difference in bulk conductivity decreases with the increase of temperature is due to the increase in the concentration of charge carriers arising from aliovalent doping. In the low temperature range, the concentration of charge carriers is determined by the thermodynamic equilibrium between the free defects and defect association pairs [16]. The linear behavior of the Arrhenius plot over a wide temperature range (150–500 °C) indicates the presence of only one type of ion conduction in these electrolyte systems. Co-doped samples showed higher conductivity than singly doped ceria suggesting that co-doping effect exists. The co-doping effect was more observable in the lower temperature region compared to the higher temperature region. For the series, $Ce_{0.9}Y_{0.1-x}M_xO_{2-\delta}$ ($x = 0$, 0.05) (M = Ca or Mg), the co-doped system exhibit better electrical properties than singly doped system, and $Ce_{0.9}Y_{0.05}Mg_{0.05}O_{1.925}$ exhibits the highest bulk conductivity (2.58×10^{-2} S/cm), grain boundary conductivity (3.13×10^{-2} S/cm) and total conductivity (1.38×10^{-2} S/cm) at 800 °C. But for the series, $Ce_{0.85}Y_{0.15-x}M_xO_{2-\delta}$ ($x = 0$, 0.05, 0.1) (M = Ca or Mg), the composition $Ce_{0.85}Y_{0.05}Ca_{0.1}O_{1.875}$ exhibits better electrical properties. The analysis of the grain boundary conductivities of the co-doped ceria system indicated an improvement of grain boundary conductivity with the increase in the concentration of Ca^{2+}, but for Mg^{2+} co-doped systems, $Ce_{0.85}Y_{0.1}Mg_{0.05}O_{1.9}$ exhibit better grain boundary conductivity.

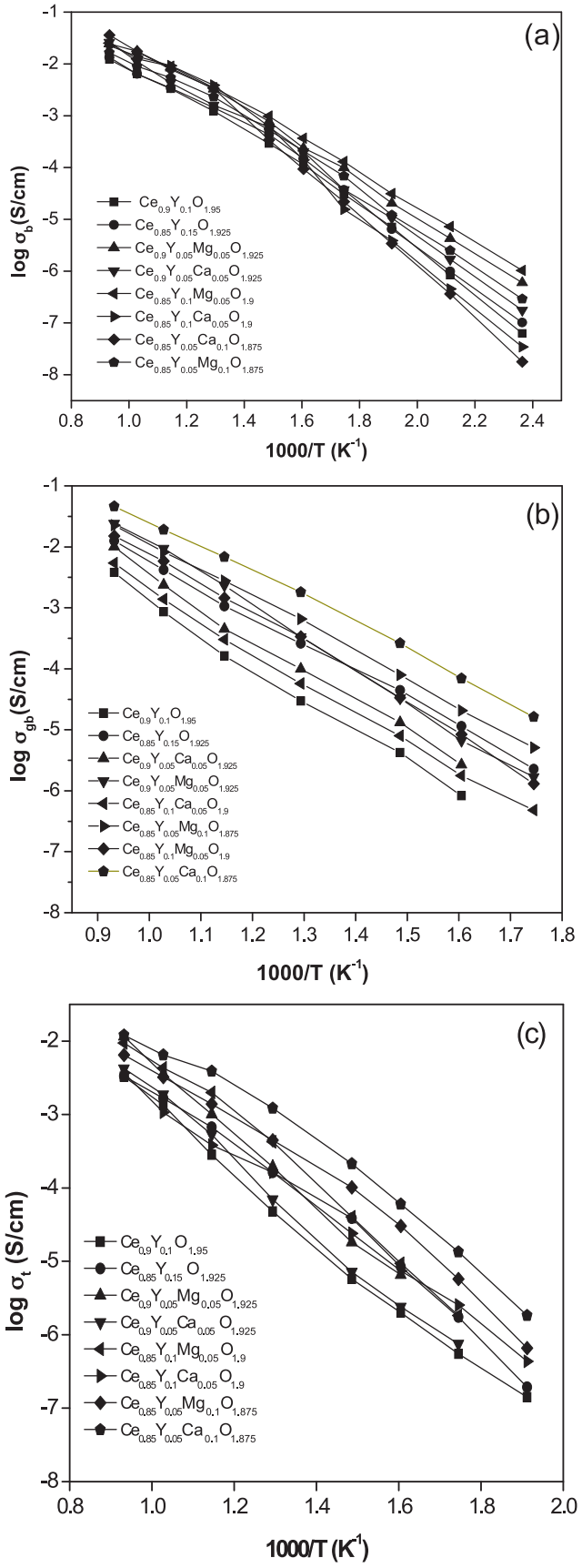

Fig. 9. The temperature dependence of bulk (a) grain boundary (b) and total (c) conductivity for single and co-doped samples.

Table 1
Bulk (σ_b), grain boundary (σ_{gb}) and total (σ_t) conductivity (S/cm) at 800 °C and activation energy (E_a) (eV) for $Ce_{0.9}Y_{0.1-x}M_xO_{2-\delta}$ (x = 0, 0.05) and $Ce_{0.85}Y_{0.15-x}M_xO_{2-\delta}$ (x = 0, 0.05, 0.1) (M = Ca or Mg) system sintered at 1500 °C for 5 h.

Composition	σ_b	σ_{gb}	σ_t	$E_{a(b)}$	$E_{a(gb)}$	$E_{a(t)}$
$Ce_{0.9}Y_{0.1}O_{1.95}$	1.19×10^{-2}	3.81×10^{-3}	2.02×10^{-3}	0.868	1.061	0.906
$Ce_{0.85}Y_{0.15}O_{1.925}$	1.35×10^{-2}	1.15×10^{-2}	3.80×10^{-3}	0.838	0.893	0.892
$Ce_{0.9}Y_{0.05}Mg_{0.05}O_{1.925}$	2.58×10^{-2}	3.13×10^{-2}	1.38×10^{-2}	0.669	1.001	0.974
$Ce_{0.9}Y_{0.05}Ca_{0.05}O_{1.925}$	2.57×10^{-2}	6.17×10^{-3}	4.98×10^{-3}	0.802	1.022	0.949
$Ce_{0.85}Y_{0.1}Mg_{0.05}O_{1.9}$	2.49×10^{-2}	1.92×10^{-2}	1.08×10^{-2}	0.680	0.962	0.869
$Ce_{0.85}Y_{0.1}Ca_{0.05}O_{1.9}$	2.19×10^{-2}	6.87×10^{-3}	5.19×10^{-3}	0.905	0.944	0.798
$Ce_{0.85}Y_{0.05}Mg_{0.1}O_{1.875}$	1.78×10^{-2}	1.51×10^{-2}	6.45×10^{-3}	0.728	0.985	0.896
$Ce_{0.85}Y_{0.05}Ca_{0.1}O_{1.875}$	3.59×10^{-2}	2.84×10^{-2}	1.59×10^{-2}	0.774	0.814	0.787

The co-doped system, $Ce_{0.85}Y_{0.05}Ca_{0.1}O_{1.875}$ shows the highest bulk conductivity (3.59×10^{-2} S/cm) and grain boundary conductivity (2.84×10^{-2} S/cm) at 800 °C out of all studied samples. Due to the two effect of bulk and grain boundary, the highest total conductivity (1.59×10^{-2} S/cm) is given by the composition $Ce_{0.85}Y_{0.05}Ca_{0.1}O_{1.875}$. For the series $Ce_{0.85}Y_{0.15-x}M_xO_{2-\delta}$ with MgO doping, the highest total conductivity (1.08×10^{-2} S/cm) is obtained for the composition $Ce_{0.85}Y_{0.1}Mg_{0.05}O_{1.9}$, further increase of MgO leads to a decrease in conductivity. This may be attributed to the very low solubility of Mg^{2+} in the $Ce_{0.85}Y_{0.15}O_{1.925}$ lattice and the segregation Mg^{2+} cations at grain boundaries with the increase in MgO dopant concentration, as can be seen in Fig. 5.

Ceria has a cubic fluorite type crystal structure and oxygen vacancies are introduced when it is doped with divalent and trivalent oxides to maintain charge balance, and these oxygen vacancies are responsible for the ionic conduction in these oxides. The formation of oxygen vacancies with the addition of yttrium and alkaline earth elements into ceria is represented by the Kröger–Vink notation as:

$$Y_2O_3 \xrightarrow{2CeO_2} 2Y'_{Ce} + 3O_o^x + V_o^{\bullet\bullet} \quad (2)$$

$$MO \xrightarrow{CeO_2} M''_{Ce} + O_o^x + V_o^{\bullet\bullet}, \quad \text{where (M = Ca,Mg)} \quad (3)$$

where Y'_{Ce} or M''_{Ce} indicate one Ce^{4+} site occupied by one Y^{3+} or M^{2+} ion. Due to coulombic attraction, defect association pairs ($Y'_{Ce} \cdot V_o^{\bullet\bullet}$, $M''_{Ce} \cdot V_o^{\bullet\bullet}$) or ($Y'_{Ce} \cdot V_o^{\bullet\bullet} \cdot Y'_{Ce}$, $M''_{Ce} \cdot V_o^{\bullet\bullet} \cdot M''_{Ce}$) are formed between the dopant and oxygen vacancies. These defect associations or complexes will prevent the oxygen vacancies from passing through the lattice and it result in a decrease of conductivity at low temperature. It can be noticed from Fig. 9(a) that the Arrhenius plot shows a significant bending which is usually interpreted as a transition from associated to dissociated behavior of the defect cluster or complex. A change in slope is observed at around 500–600 °C, and it indicates the differences in the conduction mechanism due to the changes in the behaviors of the defect at low (150–500 °C) and high (600–800 °C) temperatures and similar results were reported earlier [14]. That is in the low temperature region, activation energy equals to the migration enthalpy and defect association enthalpy, but the high temperature region is associated with only the migration enthalpy [15]. In the low temperature range, the oxygen vacancy associated with the dopant is trapped as a result of the association of defects to form defect complexes. Consequently, both association energy and migration energy of the system influence the conduction mechanism. At high temperatures, mostly all oxygen vacancies are free and the bulk conductivity is determined by the oxygen ion migration. At the same time, the difference between the bulk conductivities of single and co-doped sample decreases at high temperatures. At low dopant concentration, most of the oxygen vacancies $V_o^{\bullet\bullet}$ are probably mobile while at high dopant concentrations, defect associations localized near the dopants begin to form at the expense of oxygen vacancies [16]. From the Arrhenius plot we can see that the lowest value of bulk ionic conductivity is obtained for $Ce_{0.85}Y_{0.05}Ca_{0.1}O_{1.875}$ sample in the low temperature range, because the migration enthalpy reduces and association enthalpy increases with the increase in the addition of Ca^{2+}, however the bulk conductivity drastically increases in the high temperature range.

Fig. 9(b) shows that the grain boundary conduction increases with increasing the concentration of dopants and the maximum grain boundary conductivity is obtained for $Ce_{0.85}Y_{0.05}Ca_{0.1}O_{1.875}$ out of all the studied samples. This may be due to the change in the grain boundary contribution with the increase in dopant concentration and lowest dopant content result in lowest grain boundary conductivity. The grain boundary activation energy for the low dopant content is greater than the higher dopant content. The decrease in grain boundary activation energy with increasing the concentration of dopants is perhaps due to the presence of attractive interactions between the dopant cations and oxygen vacancies in the space charge layer leading to an increase in the number of percolation paths [16,17]. Table 1 shows for the series, $Ce_{0.85}Y_{0.15-x}Ca_xO_{2-\delta}$ (x = 0, 0.05, 0.1), the grain boundary conductivity increases as the dopant concentration increases and the composition $Ce_{0.85}Y_{0.05}Ca_{0.1}O_{1.875}$ has the highest grain boundary conductivity and lowest activation energy. It was confirmed earlier by Lei et al. [18] and Ikuhara et al. [19] that the accumulation of acceptor cations in the grain boundaries for zirconia and ceria based materials by means of electron energy loss spectroscopy (EELS) and energy dispersive X-ray spectroscopy (EDXS). Accordingly, a space charge layer model was proposed by Guo and Waser [20], it states that a grain boundary consists of a grain boundary core and two adjacent space charge layers at both sides. It has been shown that the grain boundary core of ceria is positively charged and therefore a depletion of oxygen vacancies occurs at the space charge layer [21]. The dopant cations segregate effectively at the grain boundaries as a result of the elastic strain and coulomb interactions, and it leads to the oxygen vacancy depletion at the vicinity of the grain boundaries and affect the grain boundary properties [17]. Therefore the space charge layers block the oxygen vacancies across the grain boundaries and subsequently the reduction of grain boundary conductivity. When co-doping with a very small amount, the alkaline earth element may perhaps dissolved in the grain boundary, suppressing the accumulation of Y^{3+} due to coulomb repulsion, which leads to an increase in oxygen vacancy concentration near the boundary and thus shows an improvement of grain boundary conductivity. Li et al. [22] reported an enhancement in grain boundary conductivity, when co-doped with MgO and the formation of MgO phases at the grain boundary as evidenced from XRD and FESEM to optimize the space charge regions. In our case, for Mg^{2+} co-doped series, $Ce_{0.85}Y_{0.15-x}Mg_xO_{2-\delta}$ (x = 0, 0.05, 0.1), x = 0.05 shows the better electrical properties and further increase of the amount of Mg^{2+} leads to a decrease in both bulk and grain boundary conductivity and in turn a decrease in total conductivity. This may be due to the fact that small amount of Mg^{2+} perhaps dissolved in the grain boundary restraining the accumulation of Y^{3+} due to coulomb repulsion, which increases the concentration of oxygen vacancies near the boundary and thus increases the grain boundary conductivity. When the concentration

of Mg^{2+} dopant further increases, a majority of Mg^{2+} gathered at the boundary resulting in a highly resistive phase formed at the boundaries, and it reduces the grain to grain contacts and thus decreases the conductivity. We can see from Fig. 9(b) and (c) that grain boundary conductivity has the same trend as that of the total conductivity. This is due to the fact that grain boundary makes the primary contribution to the total conductivity in polycrystalline electrolytes [23]. Other studies also reported that co-doping MgO on doped ceria system has a large influence on grain boundary than that of bulk, small addition of MgO first increases the grain boundary conductivity and further increase leads to a decreases due to the segregation of Mg^{2+} at the grain boundaries [22,24,25]. From Fig. 5, we can see that in our study the sample co-doped with Mg = 10 mole% exhibit the segregation of Mg^{2+} at the grain boundaries. Table 1 shows that the change in the grain boundary conductivity is higher than that of the bulk conductivity with the addition of alkaline earth elements, which results in an increase in the total conductivity. From Table 1, by comparing the activation energy of bulk and grain boundary, we can see that the activation energy of the grain boundary has higher values than that of the bulk, thus confirming that grain boundaries also play a major role on the activation energy of total conductivity. As reported earlier by Li et al. [17] and Pérez-Coll et al. [26], activation energy of the grain boundary is much higher than that of bulk, so the total activation energy is smaller than that of the grain boundary, and grain boundary activation energy is the dominating factor which agrees with our results.

4. Conclusions

Electrolytes of co-doped ceria with nominal compositions of $Ce_{0.9}Y_{0.1-x}M_xO_{2-\delta}$ ($x = 0, 0.05$) and $Ce_{0.85}Y_{0.15-x}M_xO_{2-\delta}$ ($x = 0, 0.05, 0.1$) (M = Ca, Mg) were prepared by mechanical milling. The X-ray diffraction patterns of all the synthesized samples confirm the cubic fluorite structure after 1 h milling and sinterization. Increasing sintering temperature helps in obtaining dense materials with better electrical properties. The dense microstructure with a wider grain size distribution was achieved after sintering at 1500 °C. Co-doping was found to enhance effectively the conductivity of the samples. In comparison to singly doped ceria, co-doping with appropriate ratio of Y^{3+} and Ca^{2+} or Mg^{2+} showed higher conductivities and lower activation energies. The effect of co-doping on the electrical properties of grain boundary was more apparent than that of the bulk. The bulk and grain boundary conductivity increases as the dopant concentration increases and the composition $Ce_{0.85}Y_{0.05}Ca_{0.1}O_{1.875}$ exhibits the highest total conductivity out of all studied samples. It implies that co-doping with optimal ratio of yttria and magnesia or calcia can further improve the electrical performance of ceria-based electrolytes.

Acknowledgment

The author R.A. Montalvo-Lozano is thankful to Conacyt, Mexico for the financial support (Grant SEP-2007-CB-84267).

References

[1] N.Q. Minh, J. Am. Ceram. Soc. 76 (3) (1993) 563.
[2] V.V. Kharton, F.M.B. Marques, A. Atkinson, Solid State Ionics 174 (2004) 135.
[3] P.-N. Huang, A. Petric, J. Electrochem. Soc. 143 (5) (1996) 1644.
[4] J. Van Herle, T. Horita, T. Kawada, N. Sakai, H. Yokokawa, M. Dokiya, J. Eur. Ceram. Soc. 16 (1996) 961.
[5] V.V. Kharton, F.M. Figueiredo, L. Navarro, E.N. Naumovich, A.V. Kovalevsky, A.A. Yaremchenko, A.P. Viskup, A. Carneiro, F.M.B. Marques, J.R. Frade, J. Mater. Sci. 36 (2001) 1105.
[6] K.P. Padmasree, R.A. Montalvo-Lozano, S.M. Montemayor, A.F. Fuentes, J. Alloys Compd. 509 (2011) 8584.
[7] M. Dudek, A. Rapacz-Kmita, M. Mroczkowska, M. Mosialek, G. Mordarski, Electrochim. Acta 55 (2010) 4387.
[8] S. Omar, E.D. Wachsman, J.C. Nino, Solid State Ionics 177 (2006) 3199.
[9] Y. Zheng, H. Gu, H. Chen, L. Gao, X. Zhu, L. Guo, Mater. Res. Bull. 44 (2009) 775.
[10] T.S. Zhang, J. Ma, S.H. Chan, P. Hing, J.A. Kilner, Solid State Sci. 6 (2004) 565.
[11] X. Guo, W. Single, J. Fleig, J. Maier, Solid State Ionics 154–155 (2002) 555.
[12] D.K. Kim, P.S. Cho, J.H. Lee, D.Y. Kim, H.M. Park, G. Auchterlonie, J. Drennan, Electrochem. Solid State Lett. 10 (5) (2007) B91.
[13] D. Pérez-Coll, D. Marrero-López, P. Núñez, S. Piñol, J.R. Frade, Electrochim. Acta 51 (2006) 6463.
[14] B. Li, Y. Liu, X. Wei, W. Pan, J. Power Sources 195 (2010) 969.
[15] H. Li, C. Xia, M. Zhu, Z. Zhou, G. Meng, Acta Mater. 54 (2006) 721.
[16] N. Cioateră, V. Pârvulescu, A. Rolle, R.N. Vannier, Solid State Ionics 180 (2009) 681.
[17] B. Li, X. Wei, W. Pan, J. Power Sources 183 (2008) 498.
[18] Y. Lei, Y. Ito, N.D. Browning, T.J. Mazanee, J. Am. Ceram. Soc. 85 (2002) 2359.
[19] Y. Ikuhara, P. Thavorniti, T. Sakuma, Acta Mater. 45 (1997) 5275.
[20] X. Guo, R. Waser, Prog. Mater. Sci. 51 (2006) 151.
[21] C. Sánchez-Bautista, A.J. Dos santos-García, J. Peña-Martinez, J. Canales-Vázques, Solid State Ionics 181 (2010) 1665.
[22] B. Li, X. Wei, W. Pan, Int. J. Hydrogen Energy 35 (2010) 3018.
[23] J.X. Zhu, D.F. Zhou, S.R. Guo, J.F. Ye, X.F. Hao, X.Q. CaO, J. Meng, J. Power Sources 174 (2007) 114.
[24] X. Hongmei, Y. Hongge, C. Zhenhua, Solid State Sci. 10 (2008) 1179.
[25] F.Y. Wang, S. Cheng, C.H. Chung, B.Z. Wan, J. Solid State Electrochem. 10 (2006) 879.
[26] D. Pérez-Coll, P. Nuñez, J.R. Frade, J.C.C. Abrantes, Electrochim. Acta 48 (2003) 1551.